Widely tunable mid-infrared quantum cascade lasers using sampled grating reflectors

Tobias S. Mansuripur,[1] Stefan Menzel,[2] Romain Blanchard,[2] Laurent Diehl,[3] Christian Pflügl,[3] Yong Huang,[4] Jae-Hyun Ryou,[4] Russell D. Dupuis,[4] Marko Loncar,[2] and Federico Capasso[2,*]

[1]*Department of Physics, Harvard University, 17 Oxford Street, Cambridge, Massachusetts 02138, USA*
[2]*School of Engineering and Applied Sciences, Harvard University, 29 Oxford Street, Cambridge, Massachusetts 02138*
[3]*Eos Photonics, 30 Spinelli Place, Cambridge, Massachusetts 02138, USA*
[4]*Center for Compound Semiconductors and School of Electrical and Computer Engineering, Georgia Institute of Technology, 777 Atlantic Dr. NW, Atlanta, Georgia 30332, USA*
[*]capasso@seas.harvard.edu

Abstract: We demonstrate a three-section, electrically pulsed quantum cascade laser which consists of a Fabry-Pérot section placed between two sampled grating distributed Bragg reflectors. The device is current-tuned between ten single modes spanning a range of 0.46 μm (63 cm^{-1}), from 8.32 to 8.78 μm. The peak optical output power exceeds 280 mW for nine of the modes.

©2012 Optical Society of America

OCIS codes: (140.5965) semiconductor lasers, quantum cascade; (140.3570) lasers, single mode

---

References and links

1. R. F. Curl, F. Capasso, C. Gmachl, A. A. Kosterev, B. McManus, R. Lewicki, M. Pusharsky, G. Wysocki, and F. K. Tittel, "Quantum cascade lasers in chemical physics," Chem. Phys. Lett. **487**(1-3), 1–18 (2010).
2. J. Faist, C. Gmachl, F. Capasso, C. Sirtori, D. L. Sivco, J. N. Baillargeon, and A. Y. Cho, "Distributed feedback quantum cascade lasers," Appl. Phys. Lett. **70**(20), 2670–2672 (1997).
3. P. Fuchs, J. Friedl, S. Höfling, J. Koeth, A. Forchel, L. Worschech, and M. Kamp, "Single mode quantum cascade lasers with shallow-etched distributed Bragg reflector," Opt. Express **20**(4), 3890–3897 (2012).
4. C. Gmachl, A. Straub, R. Colombelli, F. Capasso, D. Sivco, A. M. Sergent, and A. Y. Cho, "Single-mode, tunable distributed feedback and multiple-wavelength quantum cascade lasers," IEEE J. Quant. Elec. **38**(6), 569–581 (2002).
5. R. Maulini, M. Beck, J. Faist, and E. Gini, "Broadband tuning of external cavity bound-to-continuum quantum-cascade lasers," Appl. Phys. Lett. **84**(10), 1659–1661 (2004).
6. Y. Yao, X. J. Wang, J. Y. Fan, and C. F. Gmachl, "High performance 'continuum-to-continuum' quantum cascade lasers with a broad gain bandwidth of over 400 cm(−1)," Appl. Phys. Lett. **97**(8), 081115 (2010).
7. K. Fujita, T. Edamura, S. Furuta, and M. Yamanishi, "High-performance, homogeneous broad-gain quantum cascade lasers based on dual-upper-state design," Appl. Phys. Lett. **96**(24), 241107 (2010).
8. B. G. Lee, H. F. A. Zhang, C. Pflügl, L. Diehl, M. A. Belkin, M. Fischer, A. Wittmann, J. Faist, and F. Capasso, "Broadband distributed-feedback quantum cascade laser array operating from 8.0 to 9.8 μm," IEEE Photon. Technol. Lett. **21**(13), 914–916 (2009).
9. B. G. Lee, J. Kansky, A. K. Goyal, C. Pflügl, L. Diehl, M. A. Belkin, A. Sanchez, and F. A. Capasso, "Beam combining of quantum cascade laser arrays," Opt. Express **17**(18), 16216–16224 (2009).
10. A. K. Goyal, M. Spencer, O. Shatrovoy, B. G. Lee, L. Diehl, C. Pfluegl, A. Sanchez, and F. Capasso, "Dispersion-compensated wavelength beam combining of quantum-cascade-laser arrays," Opt. Express **19**(27), 26725–26732 (2011).
11. A. Hugi, R. Terazzi, Y. Bonetti, A. Wittmann, M. Fischer, M. Beck, J. Faist, and E. Gini, "External cavity quantum cascade laser tunable from 7.6 to 11.4 μm," Appl. Phys. Lett. **95**(6), 061103 (2009).
12. V. Jayaraman, Z. M. Chuang, and L. A. Coldren, "Theory, design, and performance of extended tuning range semiconductor lasers with sampled gratings," IEEE Jour. Quant. Elec. **29**(6), 1824–1834 (1993).
13. R. Blanchard, S. Menzel, C. Pflügl, L. Diehl, C. Wang, Y. Huang, J. H. Ryou, R. D. Dupuis, L. Dal Negro, and F. Capasso, "Gratings with an aperiodic basis: single-mode emission in multi-wavelength lasers," New J. Phys. **13**(11), 113023 (2011).
14. L. A. Coldren, US Patent # 4896325.

15. S. Slivken, N. Bandyopadhyay, S. Tsao, S. Nida, Y. Bai, Q. Y. Lu, and M. Razeghi, "Sampled grating, distributed feedback quantum cascade lasers with broad tunability and continuous operation at room temperature," Appl. Phys. Lett. **100**(26), 261112 (2012).
16. K. Boylan, V. Weldon, D. McDonald, J. O'Gorman, and J. Hegarty, "Sampled grating DBR laser as a spectroscopic source in multigas detection at 1.52-1.57 μm," IEEE Proc. Optoelect. **148**(1), 19–24 (2001).
17. Y. Huang, J.-H. Ryou, R. D. Dupuis, C. Pflügl, F. Capasso, K. Sun, A. M. Fischer, and F. A. Ponce, "Optimization of growth conditions for InGaAs/InAl/InP quantum cascade lasers by metalorganic chemical vapor deposition," J. Cryst. Growth **316**(1), 75–80 (2011).
18. A. Wittmann, T. Gresch, E. Gini, L. Hvozdara, N. Hoyler, M. Giovannini, and J. Faist, "High-performance bound-to-continuum quantum-cascade lasers for broad-gain applications," IEEE Jour. Quant. Elec. **44**(1), 36–40 (2008).

1. Introduction

Most atmospheric trace gases, including CO_2, NO, CH_4, and NH_3, have rotational-vibrational resonances in the mid-infrared (mid-IR) portion of the spectrum, typically between 3 and 16 μm. These resonances provide a unique 'fingerprint' for each molecule, which can be identified by an absorption spectroscopy experiment. While a broadband illumination source, such as a Globar, together with a Fourier transform infrared (FTIR) spectrometer can be used for this purpose, the resulting set-up is bulky and contains moving parts. Better portability and sensitivity can be achieved with a narrow linewidth, broadly tunable, high power laser source in the mid-IR, which eliminates the need for a spectrometer. Quantum cascade lasers (QCLs) are uniquely positioned to satisfy these requirements; in fact, their potential for absorption spectroscopy has already been demonstrated and commercialized [1]. Single mode emission is usually achieved by etching gratings into the waveguide to create a distributed feedback QCL (QC-DFB) [2], or by etching the grating into a section directly adjacent to the Fabry-Pérot (FP) cavity to form a distributed Bragg reflector (DBR) [3]. Wavelength tuning is achieved by exploiting the temperature dependence of the refractive index [4], either by varying the heat sink temperature or by applying a small dc bias current to cause Joule heating of the active region. In both DFB and DBR devices, the maximum fractional wavenumber tunability $\Delta k/k$ is given by the relative modal refractive index change $\Gamma\Delta n/n$, where Γ is the mode overlap factor. Typically, this results in a tuning range of no more than 5 cm^{-1} for current-induced temperature tuning. This spectral coverage is sufficient to detect a molecular absorption line of a gas species, but the large gain bandwidth of QCLs, which can reach a full width at half maximum (FWHM) of up to 600 cm^{-1} using specially designed active regions [5–7], allows for more ambitious detection schemes. A wider tuning range allows for multi-line detection, which facilitates calibration. One such scheme is the laser array [8]—a single chip that monolithically integrates thirty two QC-DFBs, each spaced apart spectrally by 9.5 cm^{-1} for a total spectral coverage of about 220 cm^{-1}. Overlapping the beams in the far field has been successfully demonstrated using wavelength beam combining with a suitable grating [9,10]. The widest spectral coverage to date has been achieved by placing a single multi-stack QCL with a bound-to-continuum active region design within an external cavity in the Littrow configuration [11], and using a rotating grating to provide wavelength-specific feedback to the QCL. The device lases in single mode over a range of 432 cm^{-1} from 7.6 to 11.4 μm. Truly continuous and mode-hop free tuning in the external cavity configuration requires broadband anti-reflection (AR) coatings with very low reflectivity and precise and active control of both the grating angle and cavity length, which constrain device portability, reliability and ruggedness.

Ideally, the full bandwidth of the QCL gain medium could be accessed continuously, one single mode at a time, in a monolithic device with a single output. This would eliminate the need for beam combining and minimize the amount of driving electronics, thereby providing a cheap, compact, robust platform for trace gas detection. We have made significant progress towards this goal through the use of a three-section QCL that consists of a standard FP gain section placed between two "sampled grating" distributed Bragg reflector (SGR) sections, a strategy that was first pursued at telecom wavelengths [12]. A schematic of the device

geometry is shown in Fig. 1(a). Our device is intended as a proof of principle that tuning can be accomplished in an electrically pulsed QCL using sampled gratings; the device differs from traditional telecom sampled grating lasers in that the reflector sections have the same active region as the gain section, there is no phase section, and the facets are not AR-coated. A SGR is essentially a DBR, except that the grating is multiplied by a sampling function. Whereas the DBR is maximally reflective over a narrow band centered at a wavenumber determined by the grating period, the sampling function introduces an additional periodicity which results in a comb of evenly spaced reflectivity peaks centered at the wavenumber determined by the non-sampled grating. A sampled grating incorporated into a single section device operated as a DFB laser can generate multi-wavelength lasing with single mode characteristics at each comb peak; the concept has even been generalized to sampled aperiodic gratings in order to suppress particular comb peaks [13].
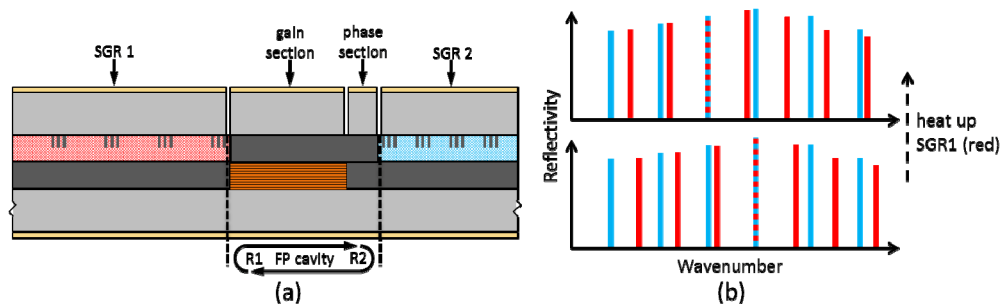

Fig. 1. (a) Schematic of a typical sampled grating DBR laser, consisting of two sampled grating reflectors (SGR) with slightly different superperiods on each side of a Fabry-Pérot (FP) cavity. The phase section controls the round-trip phase accumulation, which is critical for continuous tuning, but is not included in our device. Traditionally, the gain medium (orange) is restricted to the gain section and the facets are AR-coated, but in our device the SGRs also have gain and the facets are left uncoated. (b) Reflectivities of the SGRs and basic tuning mechanism. Light traveling in the FP cavity experiences a reflection at both SGRs whose magnitude depends on the frequency of the light. The reflectivities of the two SGRs are depicted as frequency combs (SGR1 = red, SGR2 = blue) with slightly different spacings due to the difference in the superperiods. When peaks from the two SGRs overlap at a particular frequency, the neighboring peaks do not. Therefore, light at the overlap frequency will experience a large reflection at both SGRs and have a lower lasing threshold compared to other modes. To tune the laser frequency, SGR1 is heated so that its refractive index increases and the reflectivity spectrum correspondingly shifts towards smaller wavenumbers, while SGR2 is not index tuned. The resulting alignment of the two combs is seen to cause a discrete mode hop to a mode with smaller wavenumber. (Not shown: heating SGR2 will instead cause the mode to hop to a larger wavenumber.)

True single mode emission and tuning requires the use of two SGRs, and was first described in [14] and demonstrated in [12]; very recently the concept was demonstrated in QCLs using a two-section device operating as two SG-DFB coupled cavities [15]. The two SGRs are chosen to have slightly different comb spacings so that when two of the peaks are aligned, the neighboring peaks are not. In this way, light which travels one roundtrip in the FP cavity sees the largest feedback at the wavelength for which the reflectivity peaks from the two mirrors overlap, and this condition determines the mode with the lowest lasing threshold. Discrete tuning is achieved by heating one SGR section so that its reflectivity spectrum shifts in frequency; for a small shift, two new peaks from each comb will come into alignment as shown in Fig. 1(b), causing a discrete jump in the lasing mode. This is known as Vernier tuning by analogy with the Vernier scale, which also utilizes mismatched combs [12]. This strategy overcomes the tuning limitation imposed by $\Gamma\Delta n/n$ mentioned above. To achieve quasi-continuous tuning, the two SGR sections must be heated at the same time so that both reflectivity spectra translate together in k-space. To prevent mode hops and achieve truly continuous tuning, a tunable phase section inside the FP cavity is needed to ensure that the

wavelength selected by the two SGRs also corresponds to a cavity mode satisfying the roundtrip 2π phase accumulation condition; this section is not, however, critical for demonstrating discrete tuning. Continuous tuning is still limited by the $\Gamma\Delta n/n$ factor, and so by setting the comb spacing close to one half of the maximum amount of continuous tuning, it is in principle possible to achieve wide spectral coverage through a combination of discrete jumps and continuous tuning. A more detailed description of the tuning mechanism is presented in the next section.

2. Tuning mechanism and simulations

Coupled mode theory predicts that light will be strongly reflected from a grating when the wavelength of the light is twice as large as the inverse of a spatial frequency component ($k_{grating}$) of the grating, which is the Bragg condition. To understand the relation of the Fourier components of the SGR to its design parameters, imagine constructing the SGR by beginning with an infinitely long standard $\lambda/4$ grating, as shown in Fig. 2(a). The grating consists of etched and unetched stripes of width d_e and d_u in the laser material and corresponding effective modal refractive indices n_e and n_u, where the index contrast is related to the etch depth. Ideally, the widths of the stripes are chosen to be $d_e = \lambda/(4n_e)$ and $d_u = \lambda/(4n_u)$, where λ is the vacuum wavelength of interest. The optical period of the grating is then $\Lambda_g = d_e n_e + d_u n_u$. The fundamental spatial frequency of this grating is $1/\Lambda_g$, which is plotted on the axis $k_{grating}/2$ in Fig. 2(b) to emphasize the spectral location of the reflectivity peak at $1/(2\Lambda_g)$ due to the Bragg condition. (Note: we use the standard spectroscopy notation which defines the wavenumber as $k = 1/\lambda$, without the factor of 2π.) To construct the SGR, we first multiply the grating by a top-hat function of width $N_g\Lambda_g$ which reduces the infinite grating to a finite length with N_g periods. The corresponding operation in the spectral domain is a convolution with a sinc function whose width (between first zeros) is $1/(N_g\Lambda_g)$. Second, the finite grating is convolved with a comb function whose spacing Λ_s (called the 'superperiod') is to be treated again as an optical path length, which results in a sampled grating of infinite length. The spectrum is correspondingly multiplied by a comb of spacing $1/(2\Lambda_s)$, resulting in a comb of reflectivity peaks modulated by an envelope of width $1/(N_g\Lambda_g)$ centered at $1/(2\Lambda_g)$. The final step, not shown in Fig. 2, is to multiply the infinite SGR by a top-hat function of width $N_s\Lambda_s$, so the resulting finite SGR comprises N_s superperiods. The corresponding convolution with another sinc function in the spectrum imparts a linewidth $1/(N_s\Lambda_s)$ to each comb peak. This basic understanding of the SGR parameters and reflectivity spectrum is enough to begin to design a SGR at a particular wavelength and bandwidth, and will prove very helpful in understanding the tradeoffs, such as that between tuning range and side mode suppression ratio (SMSR), that arise in design optimization. In the remainder of the paper, reflectivity spectra are calculated more accurately by modeling the grating as a one-dimensional dielectric stack with indices n_e and n_u and applying the transfer matrix method.

Finite element simulations (COMSOL) of the waveguide structure were performed to determine the modal refractive indices $n_e = 3.16$ and $n_u = 3.18$ in the etched and un-etched regions of the grating. From this, the grating stripe widths $d_e = 665$ nm and $d_u = 660$ nm were chosen to center the reflectivity spectrum of the SGRs at the peak of the electroluminescence spectrum $k = 1190$ cm^{-1} ($\lambda = 8.4$ μm). The number of grating periods $N_g = 11$ in each superperiod was chosen so that the reflectivity envelope did not vary by more than 80% over the expected tuning range. The optical path length Λ_s can be expressed in terms of physical distances as $\Lambda_s = N_g(n_e d_e + n_u d_u) + n_u L_{spacer}$, where L_{spacer} is the length of unetched region between the grating bursts of two superperiods. The spacings of the two combs, $k_1 = 3.75$ cm^{-1} and $k_2 = 4.40$ cm^{-1}, were chosen by setting $L_{spacer1} = 404.5$ μm and $L_{spacer2} = 343.5$ μm. To achieve reasonable reflectivity without the SGRs becoming excessively long, $N_s = 9$ superperiods were included in each SGR. The FP section was 2 mm long.
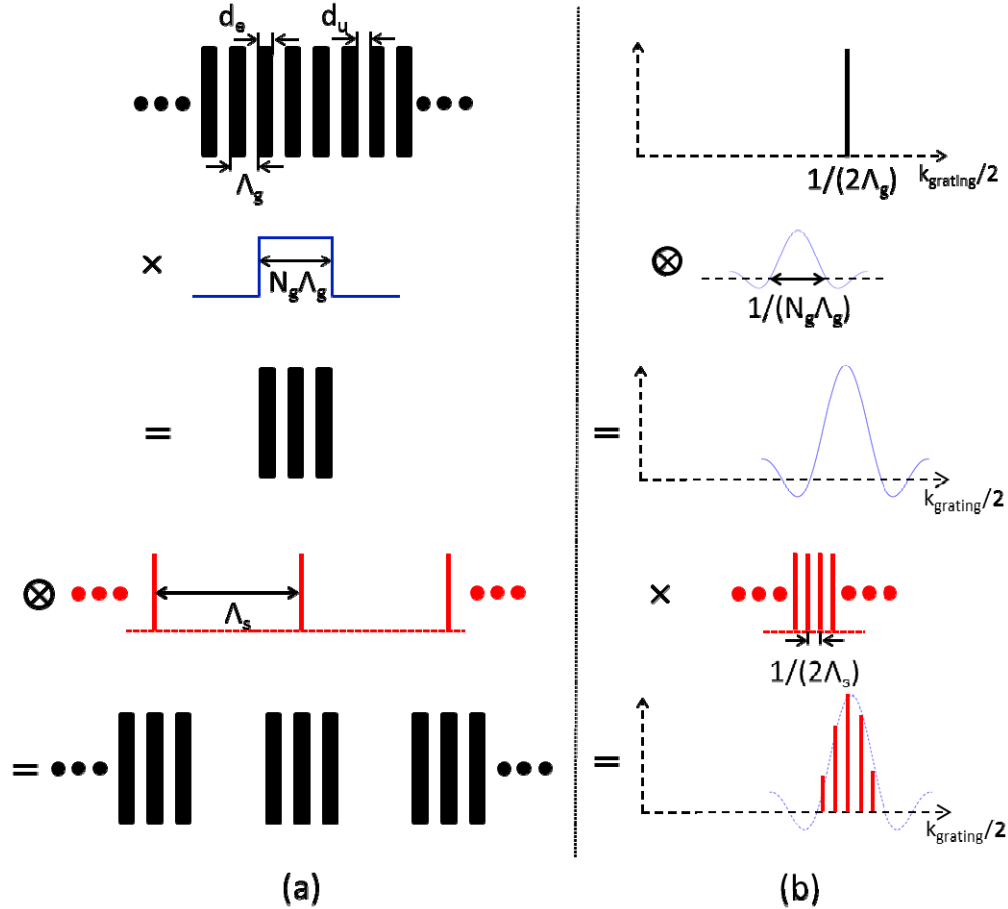
Fig. 2. The construction of a SGR and its associated Fourier components can be understood in (a) real space and (b) Fourier space. Beginning with an infinitely long DBR, a SGR is formed by multiplication with a top-hat function and convolution with a comb function. In Fourier space, the fundamental frequency of the DBR is convolved with a sinc function and multiplied by a comb function. The two periodicities Λ_g of the grating and Λ_s of the sampling manifest themselves as a comb in frequency space of spacing $1/(2\Lambda_s)$ modulated by an envelope centered at wavenumber $1/(2\Lambda_g)$ whose width between the first two zeros is $1/(N_g\Lambda_g)$, where N_g is the number of grating periods.

The simulated reflectivity spectra of both SGRs, along with the product of the two reflectivities, are shown in Fig. 3 for the grating geometries used in the experiment. From Fig. 3(a), we see the mismatch k_1-k_2 = 0.65 cm^{-1} was chosen to be slightly larger than the linewidth of the reflectivity peaks, so that when two peaks overlap strongly their nearest neighbors do not. There is a "repeat period" $k_{rep} \sim k_1 k_2/(k_1$-$k_2)$ = 26 cm^{-1} after which two additional peaks overlap, as seen in Figs. 3(b) and 3(c), but the reflectivity product is larger for the primary peaks due to the decaying envelope. In the simple Vernier tuning picture, the total amount of tuning cannot exceed k_{rep} because the peak with the largest reflectivity product will always be within $k_{rep}/2$ of the center of the envelope. One can increase k_{rep}, and thus the tuning range, by reducing the mismatch k_1-k_2, but at a cost of reducing the SMSR because the nearest neighbors of the overlapping peaks will overlap more strongly. An excellent discussion of these tradeoffs is given in [12].
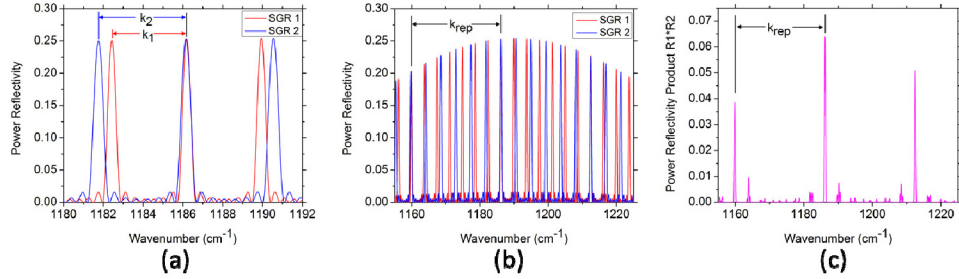
Fig. 3. (a) Simulated reflectivity spectra of the two SGRs using the experimental device parameters (with AR coatings assumed on the device facets), showing the two different comb spacing values $k_1 = 3.75$ cm^{-1} and $k_2 = 4.40$ cm^{-1}. (b) Zoomed-out view which shows the repeat spacing at $k_{rep} = 26$ cm^{-1} as well as the envelope modulation of the spectra. (c) Product of the two reflectivities which shows the modes with the largest feedback.

In the simulations shown in Fig. 3, AR-coated facets are assumed in order to more easily identify the relevant comb peaks. In the experimental device, the lack of coatings will lead to a baseline reflectivity of $|(n_u-1)/(n_u + 1)|^2 = 0.27$ which the comb sits upon. The contribution of the grating to the reflectivity (between 0.20 and 0.25 at the comb peaks) is comparable to the facet reflectivity, and therefore crucial in determining the lasing mode. The simulation also assumes that the SGRs are transparent. Because the SGRs contain the same active region as the FP section, this assumption is only strictly valid when each SGR is pumped at the transparency current, when the gain equals the waveguide loss. For smaller (larger) currents, the reflectivity will be smaller (larger) in magnitude. (If the threshold current is exceeded, however, the SGR can act as a DFB laser rather than as a reflector for the FP cavity, which is a separate matter.) In diode SG-DBR lasers, the mirror sections are regrown with passive material, and the index tuning is accomplished by electron plasma and band filling effects which result from current injection [16]. The refractive index of the QCL is much less sensitive to such effects due to the intersubband nature of the transition. Instead, we rely on thermal index tuning resulting from current-induced Joule heating. Including the active region in the SGR sections allows us to take advantage of the QCL material's ability to generate heat very efficiently.

Discrete mode hopping is achieved by tuning the refractive index of one of the mirror sections, say SGR 1, while the other remains unchanged, which translates the reflectivity spectrum of SGR1 in k-space and brings the neighboring peaks into alignment. To see why an index change results in a translation, consider a small index change from n to $n + \Delta n$ in SGR1 which results from a temperature increase in the InAlAs/InGaAs materials. This causes a small but negligible shift in the peak of the reflectivity envelope (blue curve in Fig. 2(b)). The more significant effect is the change in the optical path length of the superperiod $\Lambda_{s1} \rightarrow \Lambda_{s1} + \Delta\Lambda_{s1}$ which affects the comb spacing $k_1 \rightarrow k_1 - \Delta k_1$ where $\Delta k_1 = \Delta\Lambda_{s1}/(2\Lambda_{s1}^2)$: the entire comb (red peaks in Fig. 2(b)) contracts when the SGR is heated with the center of contraction at $k = 0$. The Nth peak—where N is an integer which counts each peak beginning at $k = 0$—shifts by an amount $N\Delta k_1$. In our particular design, we are interested only in the peaks with N between 314 and 320, which corresponds to the small spectral window of 26 cm^{-1} near $k_1 = 1190$ cm^{-1}. These few peaks shift by almost the same amount, and so the contraction manifests itself as a translation towards smaller wavenumbers. However, if one were to design a device with tuning range greater than 200 cm^{-1} then the comb contraction would be relevant and the Vernier tuning mechanism not so straightforwardly applicable. The index dispersion would also need to be accounted for, resulting in unevenly spaced comb lines.

3. Fabrication

The QCL wafer used in this experiment was grown by metalorganic chemical vapor deposition (MOCVD) on a conducting InP:S substrate [17]. The lower cladding consists of three layers: an InP layer (InP:Si, n = 1 × 10^{17} cm^{-3}, d = 3.5 μm), a thin grading layer (InGaAsP:Si, n = 1 × 10^{17} cm^{-3}, d = 30 nm), and an InGaAs layer (InGaAs:Si, n = 3 × 10^{16} cm^{-3}, d = 520 nm). Following the lower cladding, the active region comprises 35 repetitions of the heterostructure layer sequence lattice matched to InP 13/47/12/52/11/53/9/17/44/25/36/27/32/<u>27</u>/<u>25</u>/<u>28</u>/21 /31/18/34/16/39/15/42, where InGaAs wells are in plain text, AlInAs barriers are in boldface, Si n-doped layers (n = 4.9 × 10^{16} cm^{-3}) are underlined, and thicknesses are in units of angstroms. This is a bound-to-continuum design similar to the one used in [18]. The upper cladding is the same as the lower cladding but grown in reverse order. Finally, a highly doped InP layer (InP:Si, n = 5 × 10^{18} cm^{-3}, d = 500 nm) is grown on top of the upper cladding, followed by 10 nm of very highly doped InP and 20 nm of very highly doped InGaAs. The gain bandwidth was determined by electroluminescence measurements, yielding a peak at 1190 cm^{-1} and full-width at half-maximum ≈250 cm^{-1}.

The wafer processing was initiated by wet etching in an HCl:$H_2$0 (1:1) solution to remove the upper cladding layers down to the 520 nm thick InGaAs layer. The sampled gratings were defined by electron beam lithography, and etched to a depth of about 300 nm into the InGaAs layer using reactive ion etching. The original upper cladding was subsequently regrown by MOCVD to create a buried grating. Laser ridges 15 μm wide were defined by optical lithography and wet etching. An insulating silicon nitride (Si_3N_4) layer 450 nm thick was deposited using plasma-enhanced chemical vapor deposition. A window was opened into the Si_3N_4 above the laser ridge by reactive ion etching to allow for electrical contact. An electron beam evaporator was used to deposit 15 nm of titanium followed by 450 nm of gold. Adjacent sections of the device were electrically separated by leaving gaps in the metallization of length 150 μm, resulting in a contact-to-contact resistance of about 500 Ω near zero bias. The backside of the sample was then thinned to a thickness of about 150 μm, and the back contact was deposited in the same way as the top contact. The lasers were cleaved to a length of 9.1 mm (SGR1 = 4.1mm, FP = 2mm, SGR2 = 3mm). For simplicity no AR coatings were deposited on the SGR facets, although their use should drastically improve the behavior of the device. Finally, the device was indium mounted epi-side up on a copper heat sink and each section was wire bonded to a gold pad to facilitate testing.

4. Experiment

The QCL was mounted on a thermoelectric cooler held at 25°C. The light output was collected from the facet of SGR2 and sent to a FTIR spectrometer with 0.1 cm^{-1} resolution. To demonstrate the Vernier discrete tuning experimentally, one of the SGR sections needs to be controllably heated to different temperatures while the FP section and other SGR remain at constant temperature. This was done by controlling the electrical pulse widths and relative delays delivered to the different QCL sections, as shown in Fig. 4. A long "tuning pulse" of duration t_{tune} = 3 μs was delivered to one of the mirrors (SGR1 in the figure). During this time the temperature of SGR1 will rise, but the device will not lase until a short pulse of duration t_{lase} = 50 ns is applied to the FP and SGR2 sections after a time t_{del} relative to the start of the tuning pulse. The delay t_{del} was varied from 0 to 2900 ns in increments of 100 ns, with longer delays corresponding to a higher temperature in SGR1 during lasing. It was determined experimentally that t_{lase} = 50 ns was short enough to prevent the temperature of SGR1 from changing substantially during lasing and therefore prevent intra-pulse mode hops, although 50 ns is long enough to cause some linewidth broadening by intra-pulse heating. It was necessary to pulse SGR2 concurrently with the FP section in order to reduce absorption losses in SGR2 and thereby lower the lasing threshold to an experimentally accessible value. This was

achieved by electrically connecting SGR2 and the FP section with wire bonds and driving both of them with one pulser. While this configuration suffers the drawback that the current through the FP and SGR2 sections cannot be individually controlled, this turns out to not be a problem for discrete tuning. Continuous tuning can in principle be achieved by independent control of the length and delay of the pulse delivered to SGR2, allowing one to heat SGR2 controllably before lasing is initiated by pulsing the FP section. There remains the question of which current magnitudes (I_1 for SGR1, $I_{FP,2}$ for FP + SGR2) to use to optimize power output and SMSR; since there is no obvious answer a priori, we performed a large parameter sweep over six values of I_1 (from 0.41 to 1.27 A), seven values of $I_{FP,2}$ (from 0.93 to 1.96 A), and thirty values of t_{del} and recorded a spectrum at each of the 1260 driving conditions. In another experiment, the tuning pulse was applied to SGR2, while SGR1 and the FP section were electrically connected. A larger parameter sweep over 9 values of I_2 (from 0.07 to 1.42 A), 12 values of $I_{FP,1}$ (from 0.60 to 2.56 A), and 30 values of t_{del} was performed for a total of 3240 spectra. The spectra were analyzed by an automated software routine to assist in determining the optimal conditions for single mode operation.
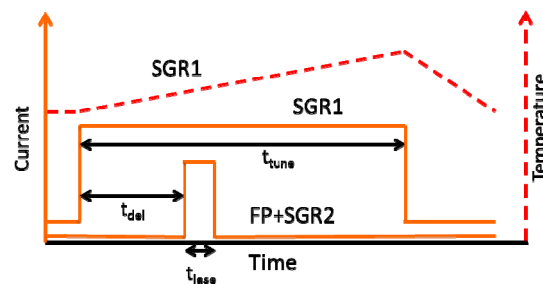

Fig. 4. Experimental approach to achieving discrete tuning. A long tuning pulse of width t_{tune} = 3 μs is applied to one of the SGR sections (SGR1 in the figure), during which time the section heats up. A short pulse of width t_{lase} = 50 ns applied to the FP section and SGR2 stimulates lasing, and the delay between the start of the two pulses is controlled by t_{del} to achieve different temperatures of SGR1 during lasing and therefore enable tuning.

Many of the recorded spectra exhibit multimode behavior—typically between two and eight weak modes—which most likely correspond to driving conditions at which none of the reflectivity peaks of the two mirrors strongly overlap within the gain bandwidth. For the driving conditions at which the reflectivity peaks do overlap well, one mode substantially dominates. In Fig. 5(a), we plot the spectra taken at I_1 = 1.27 A and $I_{FP,2}$ = 1.62 A for t_{del} = 0, 500, 800, 1700, 2200, and 2700 ns for the experiment in which SGR1 is tuned. As SGR1 is heated, the modes hop to the left in steps of k_2 = 4.40 cm^{-1} as the theory predicts. Small variations around 4.40 cm^{-1} are expected because the mode does not lase exactly at the reflectivity peak resulting from the overlap of the combs of SGR1 and SGR2, but rather at the cavity mode closest to the reflectivity peak which satisfies the roundtrip 2π phase accumulation condition. For the largest value of delay at 2700 ns, we see that the mode has jumped a large distance to the right but ends up 4.40 cm^{-1} away from the mode at 0 ns delay, which is expected due to the restriction of the tuning range to one repeat period. This particular behavior is consistent with simulations of the reflectivity product as the index change $\Delta n/n$ of SGR1 is varied from 0.25% to 0.52%, as seen in Fig. 5(b). The initial detuning of 0.25% was chosen to replicate the experimental data of four mode hops to the left followed by one to the right, and represents a small offset of the actual refractive index compared to the simulated value. Each mode hop requires an index change of about 0.06%, which corresponds to a temperature increase close to 10 K. (This value is estimated using $dn/dT = 2 \times 10^{-4}$, which is calculated based on the temperature tuning of a DFB laser at the same wavelength and made of the same material system, see Fig. 6 in [4]). As can be seen by comparing Figs. 5(a) and 5(b), the experimentally measured modes appear to be red-shifted

about 30 cm^{-1} relative to the expected peak reflectivity product from the simulations. This is not due to uncertainty in the refractive index, because the clear observation of mode hops at the designed value of 4.40 cm^{-1} suggests that the index n_u, which is largely responsible for determining the mode spacing, is quite close to the simulated value 3.18. Further investigation is required to determine the cause of the red-shift.
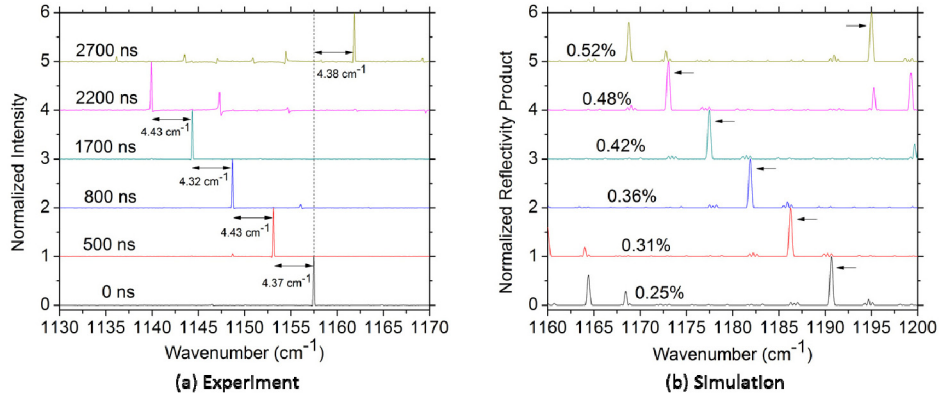

Fig. 5. (a) Spectra recorded at various values of t_{del}, indicated in the figure, for $I_1 = 1.27$ A and $I_{FP,2} = 1.62$ A, demonstrating the expected mode hops to the left in steps of $\Delta k_2 = 4.40$ cm^{-1} as SGR1 is heated. The asymmetric line shape seen in some of the side modes is an artifact from the FTIR spectrometer. (b) Simulation of the normalized reflectivity product of the two mirrors at various values of the fractional index tuning $\Delta n/n$, indicated in the figure, of SGR1. The black arrow for a particular $\Delta n/n$ indicates the wavenumber which sees the highest reflectivity, and gives an approximate indication of the mode most likely to lase if one ignores the small variation in the gain spectrum.

It is clear from Fig. 5(a) that not all modes show the same SMSR, but it is conceivable that a better SMSR can be achieved at different driving conditions. To test this, the full set of 1260 spectra was searched for single modes with SMSR exceeding 10 dB, which yielded nine distinct single modes (four of which exceed 19 dB SMSR) as shown in Fig. 6(a). All but two of the modes emit more than 300 mW of peak optical power. The black arrows point to the six modes at the locations previously seen in Fig. 5(a), spaced apart by 4.40 cm^{-1} and covering the full repeat period. Interestingly, three additional modes are found between 1170 and 1190 cm^{-1} and so the total tuning range of 47 cm^{-1} exceeds the repeat spacing; these additional modes occur for the largest value of $I_{FP,2}$ tested (1.96 A). It is clear that a complete model of these devices must take into account more than just the reflectivity of the SGR sections. If properly understood, this could open the door to device designs which exceed the repeat spacing in a controllable fashion.

In the experiment for which SGR2 was tuned rather than SGR1, the spectra collected in the parameter sweep yielded ten distinct single modes as shown in Fig. 6(b), each exceeding 13 dB in SMSR, covering a spectral range of 63 cm^{-1}. The peak power displays a clear envelope modulation, with the modes in the center exceeding 500 mW, and only the mode at the largest wavenumber emitting less than 280 mW. One pair of adjacent modes (at 1154.2 and 1157.6 cm^{-1}) exhibits a separation of 3.4 cm^{-1}, while the mean separation between the remaining pairs of adjacent modes is 7.45 ± 0.05 cm^{-1}. This separation is close to twice the expected difference of $k_1 = 3.75$ cm^{-1}. At present we cannot explain why it appears that half of the expected modes are missing, or why this nearly perfect comb of modes spaced apart by 7.45 cm^{-1} spans a bandwidth more than twice the repeat period. This large tuning range is more than a factor of 12 greater than that achieved by electrical current tuning in long-wavelength QC-DFB lasers.
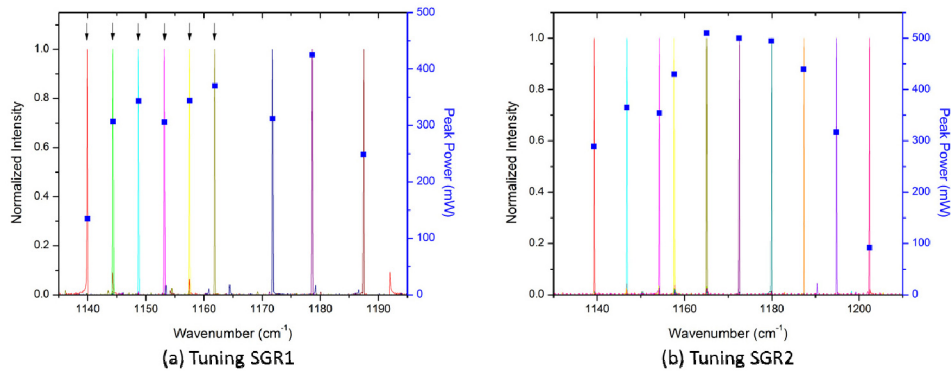
Fig. 6. Experimentally measured single modes, taken at different values of the applied currents and delay, not indicated, and individually normalized. (a) SGR1 is temperature tuned as discussed in the text. The black arrows denote the six peaks at the same locations as seen in Fig. 5(a), which span the full predicted tuning range of the device based on the simplest sampled grating theory. (b) SGR2 is tuned. The ten single modes span a range of 63 cm^{-1}.

5. Conclusion

We have fabricated a three-section sampled grating QCL and provided a clear demonstration of discrete mode hopping across the entire repeat period of 26 cm^{-1} with no missing modes. Furthermore, we have demonstrated that the device is capable of lasing at additional modes not predicted by the conventional sampled grating theory, yielding a tuning range of 0.46 μm (63 cm^{-1}), from 8.32 to 8.78 μm. By varying the driving conditions, the mode competition is determined by more factors than simply the reflectivity product of the mirrors, and lasing at additional modes is possible. More work is needed to determine whether these additional modes can be controllably and repeatably demonstrated across multiple devices. Additionally, continuous tuning should be demonstrated by heating both mirrors simultaneously, which can in principle also be achieved by a similar pulsing scheme with three independent electrical contacts. The discrete tuning range achieved in our device spans 5.4% of the center wavelength, which is larger than the recently demonstrated sampled grating DFB device that achieved a range of 2.39% around a center wavelength of 4.79 μm [15]. Additionally, the tuning mechanism we employ—namely, the adjustment of the durations and relative delays of pulses applied to various sections of the device to independently control the temperature in each section—is a robust tuning method for pulsed lasers; this method has an advantage over DC bias tuning because the magnitude of the driving current is the same for many different modes, resulting in a more consistent output power for all modes.

Acknowledgments